Optimisation of a throat downdraft gasifier for hydrogen production

Phuet Prasertcharoensuk[1], David A. Hernandez[2], Steve J. Bull[1] and Anh N. Phan[1*]

[1]School of Engineering, Newcastle University, Newcastle Upon Tyne, UK.

[2]Department of Virtual Analysis - Product Engineering FCA de México, Mexico City, Mexico.

*Corresponding authors: anh.phan@ncl.ac.uk

Abstract

Gasification of coal is a well-known technology used to convert solid coal into gas (syngas). The implementation of gasification for waste and biomass still requires attention due to the difference in nature of biomass compared to coal. Although, modification to a gasifier is one of the main approaches to achieve high quality syngas production (high H_2/CO ratio) and to eliminate tar formation, the effect of design of the gasifier has not been studied. Downdraft gasifiers are reported to produce relatively high quality syngas with low tar concentration compared to other designs. Therefore, in this study a 20 cm diameter throat downdraft gasifier was numerically optimised using Computational Fluid Dynamics modelling. The effect of throat diameter and the position of the air inlet nozzles above the throat on the properties of the gas and the temperature profile in the gasifier was systematically investigated and validated using experimental data. The throat diameter and the position of the air inlet nozzles had a significant effect on the properties of the gas and temperature profile. The modelling and experimental results agreed very well with less than 5% deviation. This confirms that the numerical approaches are valid and can be used in scaling up biomass gasification, reducing process development time from laboratory scales to pilot/industrial scales. The maximum concentration of H2

(31.2%mol) and highest H2/CO ratio (1.25) was found at a ratio of throat diameter to gasifier diameter of 0.40 and the position of the air inlet nozzles at 10 cm above the throat.

Keywords: CFD model; Biomass gasification; Throat downdraft gasifier; Syngas

1. Introduction

Global primary energy demand is expected to increase by 48% by 2040 due to the rapid growth of population, urbanization and economic activity [1]. The majority of energy supply is currently reliant on conventional energy resources such as coal (21%), petroleum (28%) and natural gas (32%) [2], which have negative environmental impacts i.e. greenhouse gas (CO_2) emissions, air pollution (SO_x, NO_x, particulates and toxic metals and other impurities) and land contamination [3]. Although, alternative energy sources (e.g. solar, hydro power, biomass, wind, geothermal and nuclear power) have been sought to reduce the dependency upon fossil fuels and reduce the environmental impact, the versatility of biomass makes it most attractive as it can be used to produce not only heat and electricity but also, chemicals and fuels for the transportation sector [4] (Figure 1). Biomass used for energy production is mostly from wood and waste wood (41%), followed by agriculture residues (24%), municipal solid waste (20%) with a small portion of energy crops (15%) [5].

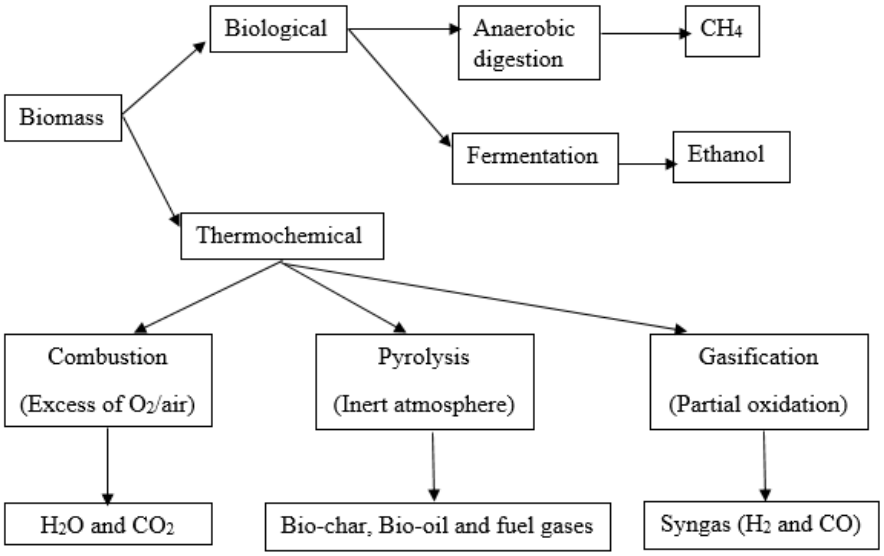

Figure 1: Biomass to bioenergy conversion pathways (adapted from Sharma et al. [6])

Gasification is a partial oxidation process to convert carbonaceous substances into a mixture of mainly H_2 and CO (synthetic gas or syngas), with small amounts of CH_4, CO_2, N_2, char, ash, tar, oils in a temperature range of 973-1773 K [7]. The proportion of components in the syngas product is strongly influenced by the type of gasifier and its operating conditions such as choice of gasifying agent (O_2, CO_2, air or steam), equivalence ratio of gasifying agent to feedstock and properties of the feedstock. Fixed-bed gasifiers are the most common technology for small and medium scale biomass gasification due to their simplicity and low investment costs compared to fluidized bed and entrained flow gasifiers [8-10]. A downdraft gasifier is preferable in this study because it is known to produce high quality syngas, with low tar content (0.015–3 g/Nm^3) in the gas stream compared to that in an updraft gasifier (30-150 g/Nm^3) [11]. Tar is a complex mixture of condensable organic compounds from the products of gasification containing primarily aromatic hydrocarbons [12-14]. The tar content influences performance of the gasification system, the quality of the product gas and creates

operational difficulties for the downstream process (e.g. corrosion, clogging and fouling of installations) [15, 16].

Computational Fluid Dynamics (CFD) modelling has previously been used to predict the behaviour of biomass gasification to optimize operating conditions of an existing gasifier [17-29]. In general, only a few aspects of the gasifier design have been investigated in any one study. For instance, some CFD studies only focused on the effect of either (i) the number and angle of nozzles [17, 30, 31] or throat angle and nozzle inclination [32-34] on the performance of a throat downdraft gasifier. Very few workers have applied CFD models for studying interactions between various design aspects of a gasifier and operating conditions to propose a proper configuration of a throat downdraft gasifier for high quality of syngas production. In this study, the effect of the ratio of throat to gasifier body diameter and the position of the air inlet nozzles above the throat were numerically investigated using CFD, ANSYS FLUENT 16.1. It is essential to examine interactions between zones in the gasifier and inlet of a gasifying agent as these determine the quality of product gas. Furthermore, the synergetic effects of gasifier design and operating conditions in a throat downdraft gasifier should be investigated to provide a correlation between operating window and the design of a downdraft gasifier for biomass gasification. Either an Eulerian-Eulerian or Eulerian-Lagrange approach could be used to resolve gas and solid phases together with the conservation equations (momentum, mass and energy) and the standard k-ε turbulence model for the gas phase. The Eulerian-Lagrange approach can track individual particles inside the system so it is suitable to study particle size distributions, interactions of particles, mass and heat transfer between particles, and transient forces acting at the particle level [35, 36], therefore it is more suitable for the modelling of fluidized bed gasifiers. The main disadvantage of the

Eulerian-Lagrange approach is it is very computationally time intensive when tracking a large number of particle collisions coupled with chemical reactions [37]. In contrast, the Eulerian-Eulerian approach assumes both gas and solid as a second continuous phase and has been proven to effectively model for fixed-bed gasifiers [38-40] in order to predict the macroscopic characteristics of a given system with low computational time. As this study mainly focused on the gas phase for syngas production from a throat downdraft gasifier instead of characterising the particles inside the gasifier, the modified Eulerian-Eulerian approach was chosen. The modelling was then validated using experimental data available in literature.

2. Numerical model of a throat downdraft gasifier

2.1 Geometry and mesh construction

A 3D model and the volume discretization of a 20 cm diameter and 55 cm long throat downdraft gasifier (Figure 2a) was created and meshed using DesignModeler (Figure 2b). The height of pyrolysis, oxidation and reduction zones were estimated at 15 cm, 10 cm and 30 cm respectively. Throat diameters of 5, 6, 8 and 10 cm were varied to obtain ratios of throat to gasifier diameter of 0.25-0.50, with varying positions of the air inlet nozzles above the throat of 8, 10 or 12 cm with the purpose of isolating the effect of both design parameters on the gas properties i.e. concentration and temperature profile. A mesh independence study was carried out at various node and cells counts and the model was built at the conditions where the solutions converged (Figure 2b).

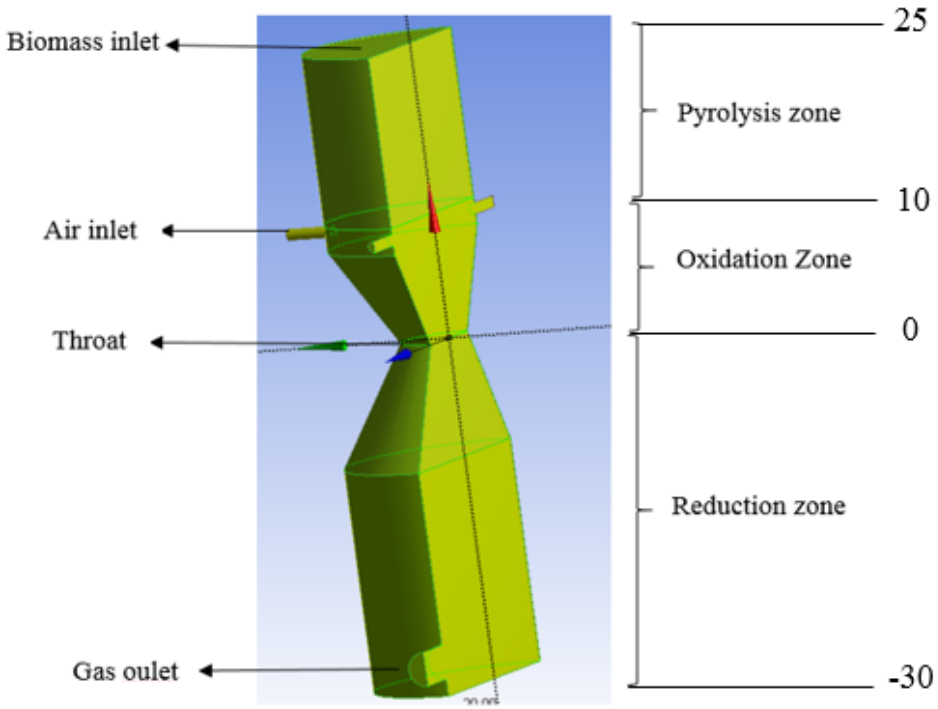

(a)

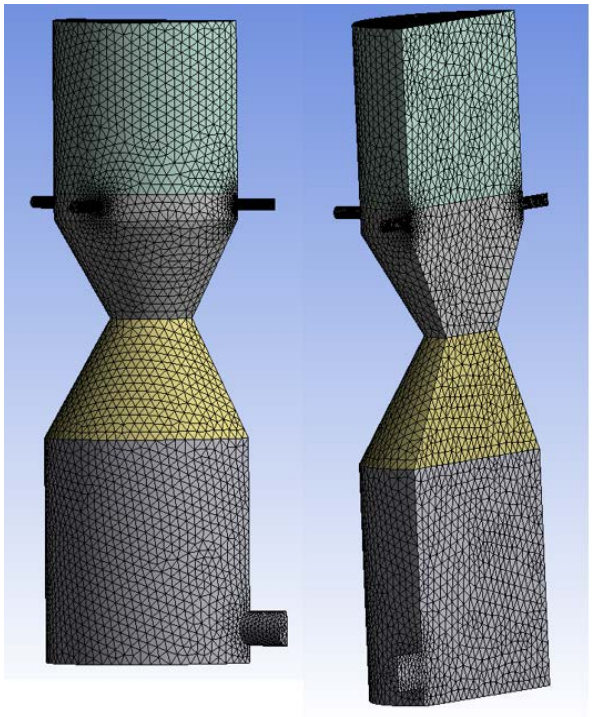

(b)

Figure 2: (a) Configuration of the throat downdraft gasifier; (b) Mesh model of the throat downdraft gasifier.

2.2 Computational model

Computational Fluid Dynamic (CFD) software, ANSYS FLUENT 16.1 was used for numerical simulation in this study. The main objective of the CFD analysis was to obtain accurate and reliable modelling results in a reasonable computational time to enable design optimisation. The species transport solution is solved by using the pressure based solver under gravitational acceleration. The Eulerian-Eulerian approach was used to solve transport phenomena, with the conservation of momentum, mass and energy equations. The standard k-ε model was used to capture the turbulence flow of the gas phase inside the gasifier with the standard wall functions. The SIMPLE algorithm scheme was used to solve the pressure-velocity coupling and the standard scheme was chosen for the pressure discretization. The second order upwind scheme was implemented after grid independence studies were completed to obtain accurate results for other calculated variables.

2.2.1 Model assumptions

To simplify the simulation of a throat downdraft gasifier, the following assumptions were made:

- Atmospheric pressure.
- The gasifier was operated under steady state conditions.
- No heat loss through the vessel wall.
- No-slip boundary condition at the wall of the gasifier. The wall was assumed to be insulated and the heat flux at the wall was neglected.
- The wood feed rate was 1 $kghr^{-1}$ at a temperature of 400 K with the moisture content less than 10 %wt. The drying zone was not included in the gasifier

configuration but it was assumed that the feedstock would achieve moisture content <10 %wt when it reached the pyrolysis zone.

- The gasifying agent (air) was introduced through nozzles at 350 K
- The ratio of the actual air/fuel to the stoichiometric air/fuel (ER ratio) was fixed at 0.25.

2.2.2 Governing equations

2.2.2.1 The momentum conservation equation

The momentum equation based on the Newton's laws of motion, relates the sum of the forces acting on a fluid element to its acceleration which is the rate of change of momentum in the direction of the resultant force. The momentum conservation equation can be written in the following form:

$$\frac{\partial}{\partial t}(\rho\vec{v}) + \nabla.(\rho\vec{v}\vec{v}) = -\nabla p + \nabla.(\tau) + \rho\vec{g} + \vec{F} \quad (2.1)$$

where ρ is the static pressure, $\rho\vec{g}$ and $\vec{F}$ are the gravitational body force and external body force respectively. The stress tensor τ in Equation 2.1 is defined by:

$$\tau = \mu\left[(\nabla\vec{v} + \nabla\vec{v}^T) - \frac{2}{3}\nabla.\vec{v}I\right] \quad (2.2)$$

where I is the unity matrix and $\vec{v}^T$ is the transpose of $\vec{v}$

2.2.2.2 The mass conservation equation

The general form of the mass conservation equation, known as the continuity equation is written as follows:

$$\frac{\partial\rho}{\partial t} + \nabla.(\rho\vec{v}) = S_m \quad (2.3)$$

where S_m is the mass added to the continuous phase from the dispersed second phase.

2.2.2.3 The energy conservation equation

The energy conservation is based on the first law of thermodynamics, the internal energy gained by a system must be equal to the heat absorbed by the system minus work done by the system. It can be written in the general form as follows:

$$\frac{\partial}{\partial t}(\rho E) + \nabla.\left(\vec{v}(\rho E + p)\right) = \nabla.\left(k_{eff}\nabla T - \sum_{j=1}^{N} h_j \vec{J}_j + (\tau.\vec{v})\right) + S_h \quad (2.4)$$

where k_{eff} is the effective thermal conductivity (k + k_t, where k_t is the turbulent thermal conductivity). The first three terms of the right hand side of the Equation 2.4 represent heat flux due to the conduction according to Fourier's law of conduction, species diffusion and viscous dissipation due to normal shear stresses respectively. The total energy E in Equation 2.4 can be defined by:

$$E = h - \frac{p}{\rho} + \frac{v^2}{2} \quad (2.5)$$

where the enthalpy is defined as:

$$h = \sum_{j=1}^{N} Y_j h_j \quad (2.6)$$

with Y_j being the mass fraction of species j and

$$h_j = \int_{T_{ref}}^{T} c_{p,j}\, dT \quad (2.7)$$

where the value used for T_{ref} in the sensible enthalpy for the pressure-based solver is 298.15 K

2.2.2.4 Transport equation for standard k-epsilon

The standard k-ε model is one of the most used turbulence models in Computational Fluid Dynamics due to its robustness and reasonable accuracy for a wide range of flows. The k-ε model is a semi empirical model based on transport equations for turbulent kinetic energy k and its dissipation rate ε. In the derivation of the model it is assumed that the

flow is fully turbulent and the effects of molecular viscosity are negligible. The transport equations for turbulent kinetic energy and its dissipation rate are defined as follow:

$$\frac{\partial}{\partial t}(\rho k) + \frac{\partial}{\partial x_i}(\rho k u_i) = \frac{\partial}{\partial x_j}\left[\left(\mu + \frac{\mu_t}{\sigma_k}\right)\frac{\partial k}{\partial x_j}\right] + G_k + G_b - \rho\varepsilon - Y_m + S_k \quad (2.8)$$

$$\frac{\partial}{\partial t}(\rho \varepsilon) + \frac{\partial}{\partial x_i}(\rho \varepsilon u_i) = \frac{\partial}{\partial x_j}\left[\left(\mu + \frac{\mu_t}{\sigma_\varepsilon}\right)\frac{\partial \varepsilon}{\partial x_j}\right] + C_{1\varepsilon}\frac{\varepsilon}{k}(G_k + C_{3\varepsilon}G_b) - C_{2\varepsilon}\rho\frac{\varepsilon^2}{k} + S_\varepsilon \quad (2.9)$$

where S_k and S_ε are the source terms for k and ε respectively and G_k is the term for the production of turbulent kinetic energy due to the mean velocity gradient and the Reynolds stress is defined as:

$$G_k = -\rho\overline{u_i' u_j'}\frac{\partial u_j}{\partial x_i} \quad (2.10)$$

G_b represents the generation of turbulent kinetic energy that arises due to buoyancy and is defined as follows:

$$G_b = \beta g_i \frac{\mu_t}{Pr_t}\frac{\partial T}{\partial x_i} \quad (2.11)$$

Y_M represents the contribution of the fluctuating dilatation in compressible turbulence to the overall dissipation rate and is defined as:

$$Y_M = 2\rho\varepsilon M_t^2 \quad (2.12)$$

The turbulent viscosity (μ_t) is computed by combining the local values of turbulent kinetic energy (k) and dissipation rate (ε) at each point by:

$$\mu_t = \rho C_\mu \frac{k^2}{\varepsilon} \quad (2.13)$$

The values of $C_{1\varepsilon}$, $C_{2\varepsilon}$, C_μ, σ_k and σ_ε in Equations 2.8 and 2.9 are constants and their values for the standard k-ε model are follows:

$C_{1\varepsilon}$ = 1.44, $C_{2\varepsilon}$ = 1.92, C_μ = 0.09, σ_k = 1.00 and σ_ε = 1.30

2.2.3 Reactions model

2.2.3.1 The pyrolysis zone

Pyrolysis is the thermochemical decomposition of feedstock to condensable and non-condensable gases and char, in the absence of oxygen/air at a temperature range of 473-773 K [41]. The overall pyrolysis decomposition can be described in Figure 3 below.

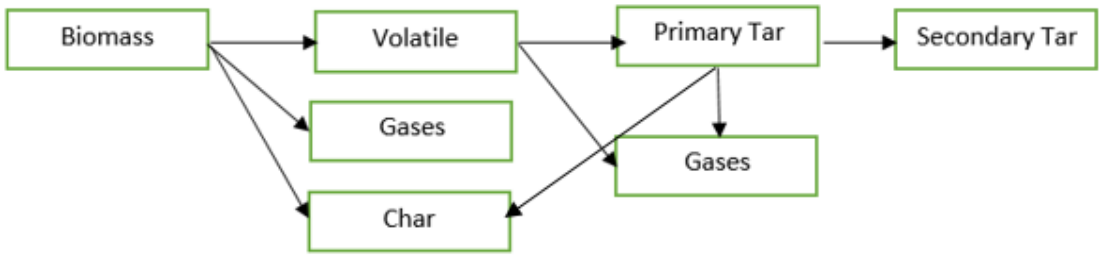

Figure 3: Reaction pathways in the pyrolysis stage (adapted from Fernando and Narayan [42])

There is limited kinetic reaction data available in the literature to represent the exact mechanisms of the pyrolysis process (Figure 3). This is mainly due to the large number of possible reactions occurring in the pyrolysis zone of which can generate tars. Tars are a complex mixture of condensable hydrocarbons containing single, multiple ring aromatic compounds with and without complex polycyclic aromatic hydrocarbons (PAHs) [43-45]. A simple one-step global reaction model has been widely accepted to model the pyrolysis processes reactions developed by Di Blasi [46, 47] and Fernando et al. [48]. This model assumes that all the volatiles and tar compounds in the pyrolysis stage are instantaneously decomposed further into CO, CO_2, CH_4, H_2 and H_2O compounds to simplify the model. Kinetic parameters for pyrolysis e.g. pre-exponential and activation energy was 1.00×10^8 s^{-1} and 140 $kJmol^{-1}$ respectively [19, 49].

2.2.3.2 The oxidation zone

The oxidation zone is where the reactions between char from the pyrolysis stage and the gasifying agent (O_2, CO_2, air or steam) occur at a temperature between 1373-1773 K to generate most of the CO, H_2O and CO_2 [50]. Three main reactions in the oxidation zone are considered with their kinetic reaction rate parameters that were used in the model listed in Table 1.

$$C + O_2 \rightarrow CO_2 \ (\Delta H = -394 \text{ kJkmol}^{-1}) \quad \text{(R-1)}$$

$$C + \frac{1}{2}O_2 \rightarrow CO \ (\Delta H = -110 \text{ kJkmol}^{-1}) \quad \text{(R-2)}$$

$$H_2 + \frac{1}{2}O_2 \rightarrow H_2O \ (\Delta H = -242 \text{ kJkmol}^{-1}) \quad \text{(R-3)}$$

2.3.2.3 The reduction zone

In this zone the remaining residues and gaseous products from the pyrolysis and oxidation zones are converted into non-condensable gases (H_2, CO, CO_2, CH_4) in a temperature range of 973-1273 K including both heterogeneous and homogeneous reactions [7, 8]. Five reactions are considered in the reduction zone as follows and the kinetic reaction rate parameters used in the model are listed in Table 1.

$$C + CO_2 \rightarrow 2CO \ (\Delta H = +172 \text{ kJkmol}^{-1}) \quad \text{(Boudouard reaction)} \quad \text{(R-4)}$$

$$C + H_2O \rightarrow CO + H_2 \ (\Delta H = +131 \text{ kJkmol}^{-1}) \quad \text{(steam reforming reaction)} \quad \text{(R-5)}$$

$$C + 2H_2 \rightarrow CH_4 \ (\Delta H = -74.8 \text{ kJkmol}^{-1}) \quad \text{(hydrogenation reaction)} \quad \text{(R-6)}$$

$$CH_4 + H_2O \rightarrow CO + 3H_2 \ (\Delta H = +206 \text{ kJkmol}^{-1}) \quad \text{(steam reforming reaction)} \quad \text{(R-7)}$$

$$CO + H_2O \rightarrow CO_2 + H_2 \ (\Delta H = -41.2 \text{ kJkmol}^{-1}) \quad \text{(water-gas shift reaction)} \quad \text{(R-8)}$$

2.2.4 Boundary conditions and solution methods

It was assumed that waste wood was fed from the top of the gasifier at a constant rate of 1 $kghr^{-1}$ at a temperature of 400 K (Figure 2). The model assumed that the waste wood passed through the drying zone, which was separated from the configuration of the

downdraft gasifier setup in Figure 2. The assumption is accepted as in reality feedstock must be dried to a certain moisture content before feeding into a gasifier. The physiochemical characteristics of the wood were experimentally determined and the kinetic parameters in the gasification process were adapted from literature values. The gasifying agent (air) was preheated to 350 K and then introduced into the gasifier through four inlet nozzles, which are located at the middle part of the gasifier (Figure 2a) at a fixed ratio of the actual air/fuel to the stoichiometric air/fuel (ER ratio) of 0.25. The numerical methods and boundary conditions used in this model are shown in Table 1.

Table 1: Parameters used for modelling a throat downdraft gasifier

Properties of wood	
Proximate analysis	Values (%wt, dry basis)
Volatile matter	84.12
Fixed carbon	15.37
Ash	0.51
Ultimate analysis	Values (%wt, dry basis)
C	41.80
H	6.39
O	51.50
N	0.32
Low heating value ($MJkg^{-1}$)	15.27
High heating value ($MJkg^{-1}$)	17.69
The empirical formula of wood	$C_{6.00}H_{10.50}O_{5.00}N_{0.05}$
Kinetic reaction rates occurred in gasification process [19]	

Reaction	Pre-exponential factor (s^{-1})	Activation energy ($kJmol^{-1}$)
$\text{Biomass} \rightarrow \text{Char} + \text{ash} + \text{volatiles}\ (H_2, CO, CH_4, CO_2, H_2O)$	1.00×10^8	1.40×10^2
$C + O_2 \rightarrow CO_2$	5.67×10^9	1.60×10^2
$C + \frac{1}{2}O_2 \rightarrow CO$	7.92×10^4	2.18×10^2
$H_2 + \frac{1}{2}O_2 \rightarrow H_2O$	3.53×10^8	3.05×10^1
$C + CO_2 \rightarrow 2CO$	5.89×10^2	2.23×10^2
$C + H_2O \rightarrow CO + H_2$	5.71	6.58×10^1
$C + 2H_2 \rightarrow CH_4$	1.00×10^{11}	4.20×10^1
$CH_4 + H_2O \rightarrow CO + 3H_2$	7.30×10^1	3.62×10^1
$CO + H_2O \rightarrow CO_2 + H_2$	3.00×10^{-2}	6.58×10^1

Boundary conditions

Zone	Boundary type	Value	Temperature (K)
Air inlet	Velocity inlet	1.73 ms^{-1}	350
Biomass inlet	Mass flow inlet	2.77×10^{-4} kgs^{-1}	400
Gas outlet	Pressure outlet	0 Pa	700
Symmetry	Symmetry	-	-
Gasifier wall	Wall	0 Wm^{-2}	-

Solution methods	
Pressure-Velocity Coupling	SIMPLE
Gradient	Least Squares Cell Based
Pressure	Standard
All other parameters	Second Order Upwind
Solution Controls	
Under-Relaxation Factors	
Pressure	0.3
Density	1
Body Forces	1
Momentum	0.7
Turbulent Kinetic Energy	0.8
Turbulent Dissipation Rate	0.8
Turbulent Viscosity	1
Energy	1
Temperature	1
Mean Mixture Fraction	1
Mixture Fraction Variance	0.9
Discrete Phase Sources	0.5
Solution Initialization	
Initialization Method	Hybrid Initialization
Run Calculation	
Number of Iterations	1500

3. Results and discussion

3.1 Effect of throat to gasifier diameter: modelling results and validation

3.1.1 Syngas composition

The formation of syngas in the throat downdraft gasifier with a throat diameter 5, 6, 8 and 10 cm (or ratios of throat to gasifier diameter of 0.25-0.50) at a fixed position of the air inlet nozzles at 10 cm above the throat is illustrated in Figure 4. The results showed that the throat diameter had a significant impact on the formation of syngas across the throat downdraft gasifier. The H_2 and CO formation was high in the reduction zone (28-31%mol H_2 and 25-32%mol CO) compared to that in pyrolysis and oxidation zones. This is due to the Boudouard (R-4), water gas (R-5) and steam-reforming (R-7) reactions occurring in this zone. The CO_2 concentration was low in the pyrolysis zone (5-11%mol) but increased to 21-27%mol in the oxidation zone. This increase is due to the combustion of volatiles and char (R-1) and others. A decrease in CO_2 in the reduction zone to ~14%mol could be due to the Boudouard reaction (R-4). The CH_4 concentration was maximised in the pyrolysis zone at 17-18%mol and further reduced in the oxidation and reductions zones to 3-5%mol, due to the steam-reforming reaction (R-7).

A uniform formation of syngas across the throat downdraft gasifier was observed at a ratio of throat diameter to gasifier diameter of 0.40 (Figure 4c). This is due to a good proportion of the ratio of throat diameter to gasifier diameter and the air velocity inlet, resulting in well-mixed volatiles and gasifying agent (air) which produced uniform concentration of product gas across the throat downdraft gasifier. This sizing of the gasifier also enhanced temperature uniformity in the oxidation zone (Figure 6c). High and uniform temperature (1800-2000 K) in the oxidation zone could eliminate the tar formation in the gas stream to achieve high quality of syngas production. The main syngas

composition generated under the various designs at a fixed position of the air inlet nozzles at 10 cm above the throat is illustrated in Table 2.

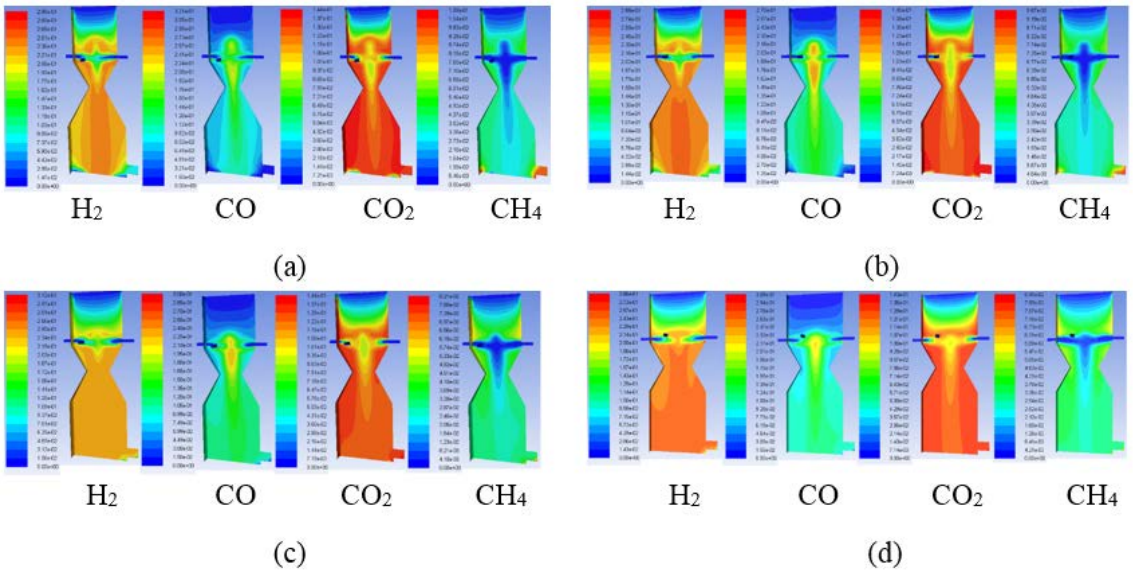

Figure 4: Gas profiles at a ratio of throat to gasifier diameter of (a) 0.25; (b) 0.30; (c) 0.40 and (d) 0.50 at a fixed position of the air inlet nozzles at 10 cm above the throat

Table 2: Modelling gas composition at the outlet over various throat diameters at a fixed position of the air inlet nozzles at 10 cm above the throat

Syngas composition (%mol)	Throat diameter, cm (ratio of throat to gasifier diameter)			
	5 (0.25)	6 (0.30)	8 (0.40)	10 (0.50)
H_2	29.49	28.79	31.23	28.58
CO	32.06	27.04	24.99	25.92
CO_2	14.41	14.47	14.38	14.28
CH_4	5.92	4.67	3.20	3.41

As shown in Table 2, the throat diameter had a considerable effect on the H_2/CO ratio and CH_4 concentration, but little influence on the CO_2 concentration in the syngas. The H_2

concentration at the outlet (31.2%mol) maximised at a ratio of throat to gasifier diameter of 0.40 and decreased when increasing the ratio of throat to gasifier diameter. The concentration of CO_2 remained almost constant around 14.4%mol with all tested throat to gasifier diameter ratios. However, CH_4 concentration decreased from 5.90%mol to 3.41%mol when increasing the ratio of throat to gasifier diameter from 0.25 to 0.50. The uniform temperature across the throat downdraft gasifier (Figure 6), favours the products of endothermic reactions, i.e. the Boudouard (R-4), water gas (R-5) and steam-reforming (R-7) reactions, resulting in an increased concentration of H_2 and CO. Moreover, an increase in the steam-reforming reaction (R-7) also resulted in a decrease of CH_4 concentration in the gas stream. The gas concentrations obtained from this study (Table 2) were slightly higher than other modelling studies [21, 24, 32, 51-53]. Previous modelling studied showed that the syngas composition generated from the throat downdraft gasifier are in the range of 13-25%mol H_2, 18-38%mol CO, 8-11%mol CO_2 and 1-3%mol of CH_4. The differences were due to the assumptions, kinetic parameters, properties of feedstock and/or gasifier design.

Comparing to experimental data of a small scale throat downdraft gasifier [21, 29, 54, 55] (the designs and operating parameters were shown in Table 3), the trends of syngas composition and temperature profile was similar. As shown in Figure 5, the ratio of H_2/CO increased from 0.56 to 0.86 when increasing the ratio of throat to gasifier diameter from 0.25 to 0.41 and then decreased with a further increase in the ratio of throat to gasifier diameter to 0.65 at 0.45. A similar trend was also observed with CO_2 concentration. A reduction in the concentration of CH_4 was observed when increasing the ratio of throat to gasifier diameter. The gas composition obtained from the modelling results of this study (Table 2) and experimental data shows the same trends with

approximately 4.62% difference across the range. It is also noted that the concentration of syngas from this study was slightly higher than that obtained from experimental data. This is because (i) the simulation model assumed that all the volatiles and tar compounds in the pyrolysis zone were instantaneously decomposed into CO, CO_2, CH_4, H_2 and H_2O compounds, (ii) the simulation model leads to more effective gasification reactions, in terms of kinetic reaction rates compared to experimental, (iii) the equivalence ratio (ER) and the composition of biomass feedstock were used and (iv) no heat loss in the system was assumed, resulting in an increased proportion of components in the syngas product.

Table 3: The experimental designs and operating parameters of a throat downdraft gasifier

	Zainal et al. [29]	Chawdhury and Mahkamov [54]	Duleeka et al. [55]	Ozgun and Mehmet [21]
Fuel and composition (%wt, dry basis)	Wood chip: (47.3% C; 5.8% H; 46.1% O; 0.8% N)	Wood chip: (54.0% C; 6.0% H; 43.0% O)	Wood stick: (48.6% C; 6.2% H; 44.87% O; 0.33% N)	Wood pellets: (50.67% C; 6.18% H; 41.15% O; 2% N)
Biomass feed rate ($kghr^{-1}$)	n.a.	3.1	1.0	3.5-4.0
Particle diameter (cm)	5	3-7	2.5	1

Gasifier dimensions (H/Ø) (cm)	250/60	91.7/21.9	110/39	55/28
Throat diameter (cm)	20	8.8	17.5	7
Throat to gasifier ratio	0.33	0.40	0.45	0.25
Equivalence ratio (ER)	0.27	0.35	0.36	0.23

315

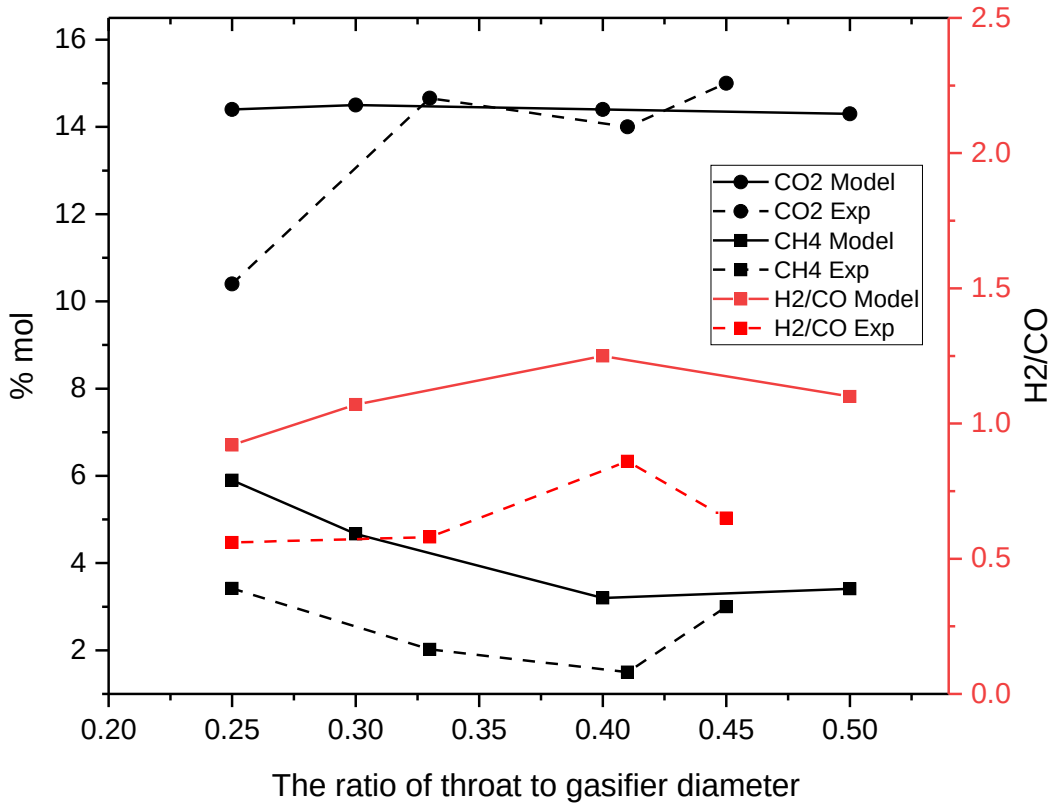

316

317 Figure 5: Comparison of modelling gas composition obtained from this study and

318 experimental data derived from literature [21, 29, 54, 55].

3.1.2 Temperature profile

The temperature distribution across the throat downdraft gasifier over various throat diameters of 5, 6, 8 and 10 cm, corresponding to the ratios of throat to gasifier diameter of 0.25-0.50 at a fixed position of the air inlet nozzles of 10 cm above the throat are illustrated in Figure 6. It can be observed that between 10 cm and 25 cm, corresponding to the pyrolysis zone (shown in Figure 2a), the temperature increased from 400 K to 1100 K. This is due to the heat provided by the radiation from the oxidation zone (combustion of char), which is the hottest part of the throat downdraft gasifier [8, 50, 56]. However, no significant changes in the temperature distribution in the pyrolysis zone were observed under any of the tested throat diameters. The oxidation zone occurred at the height of 0 cm to 10 cm in the gasifier (Figure 2a). This is important as this is the region where the main reactions occur in the throat downdraft gasifier; in consequence the relationship between throat diameter, gasifier diameter and the position of the air inlet nozzles has an effect on the temperature distribution and the properties of the syngas. As shown in Figure 6, the high and uniform temperature of 2000 K across the oxidation zone was observed with a ratio of throat to gasifier diameter of 0.40 (Figure 6c) compared to at a ratio of 0.25 and 0.30 at 1800 K and 0.50 at 1600 K. High and uniform temperature across the oxidation zone is important to eliminate tar formation in the gas stream [7, 57, 58]. The reduction zone at distance of 0 cm to -30 cm (Figure 2a), had temperature in the range of 900-1000 K with all tested throat to gasifier diameter ratios. Syngas (H_2 and CO) was produced in this region via the reactions R-4-8.

The trend of modelling temperature distribution in three different zones (pyrolysis, oxidation and reduction) agreed very well with experimental data derived from the literature [21, 29, 54, 55]: increasing from pyrolysis zone to oxidation zone and then

decreasing gradually. The differences between the modelling temperature in the pyrolysis and reduction zones and those obtained from experiments was less than 10%. However, the modelling temperature in the oxidation zone was up 36% higher. This can be due to (i) the assumption made in the model air was preheated at 350 K before introduction into the gasifier through four nozzles, (ii) no heat loss in the system, (iii) rates of reactions occurring in the oxidation zone and (iv) the ratio of the actual air/fuel to the stoichiometric air/fuel (ER ratio) i.e. at high ER ratio leading to an increase in the gasification temperature particularly in the oxidation zone [10, 59]. High and uniform temperature across the throat downdraft gasifier was obtained at a ratio of throat diameter to gasifier diameter of 0.40.

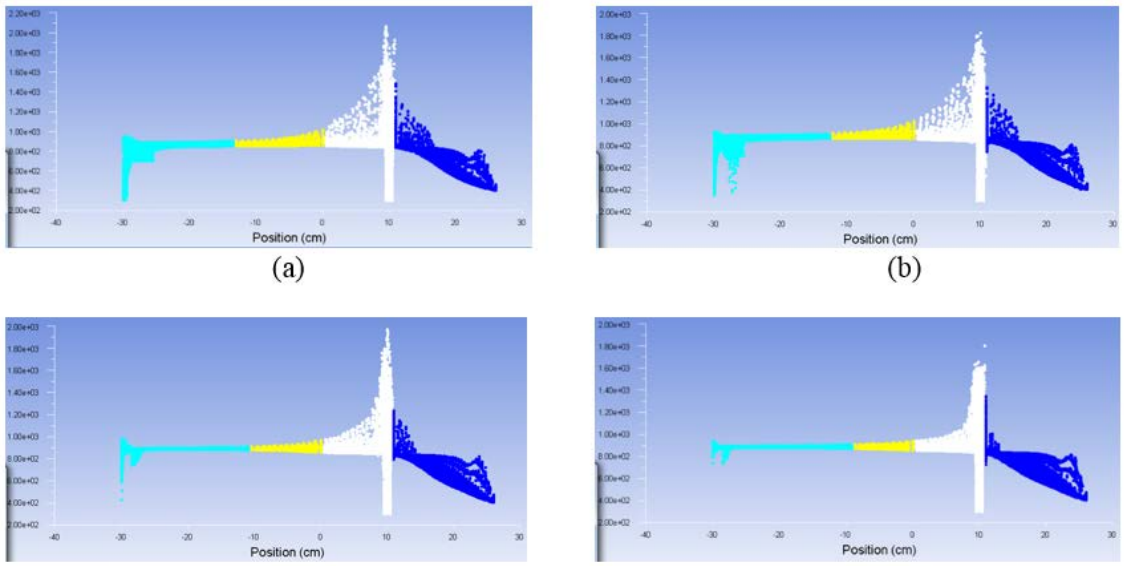

Figure 6: Temperature distribution at a ratio of throat to gasifier diameter of (a) 0.25; (b) 0.30; (c) 0.40 and (d) 0.50 at a fixed position of the air inlet nozzles at 10 cm above the throat

357 **3.2 Effect of the air inlet nozzles position above the throat: modelling results and**
358 **validation**

359 **3.2.1 Syngas composition**

360 The formation of the produced gas in a throat downdraft gasifier under various air inlet
361 nozzles positions located at 8, 10 and 12 cm above the throat at a fixed throat to gasifier
362 diameter ratio of 0.40 are illustrated in Figure 7. H_2 and CO concentrations were
363 maximised in the reduction zone in the range of 27-31%mol H_2 and 23-27%mol CO, via
364 the Boudouard (R-4), water gas (R-5) and steam-reforming (R-7) reactions. The CO_2
365 concentration was low (6-10%mol) in the pyrolysis zone and maximised at 23-27%mol
366 in the oxidation zone, due to the combustion of char (R-1) followed by a decrease to
367 ~14%mol after passing through the reduction zone. A similar trend was observed with
368 the CH_4 concentration. As shown in Figure 7, the formation of syngas was more uniform
369 across the throat downdraft gasifier at the position of the air inlet nozzles at 10 cm (Figure
370 7b) and 12 cm (Figure 7c) than at 8 cm above the throat (Figure 7a). When the air inlet
371 nozzles were positioned at 8 cm above the throat, they sat at the beginning of the
372 inclination of the throat, therefore cold spots may occur resulting in low and non-uniform
373 temperature with poor mixing of the volatiles, char and gasifying agent (air) in the
374 oxidation zone. A comparison of the main syngas compositions generated under the
375 various air inlet nozzles positions above the throat at a fixed throat to gasifier diameter
376 ratio is illustrated in Table 4.
377

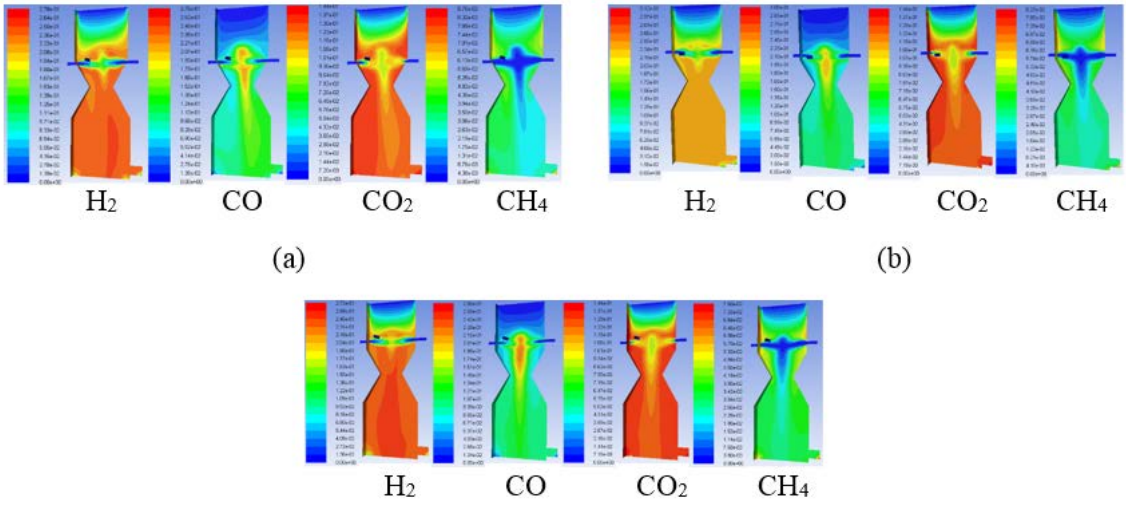

Figure 7: Gas profiles at the air inlet nozzles position at (a) 8 cm; (b) 10 cm and (c) 12 cm above the throat at a fixed throat to gasifier diameter ratio of 0.40

Table 4: Gas composition at the outlet over various air inlet nozzles positions above the throat at a fixed throat to gasifier diameter ratio of 0.40

Syngas composition (%mol)	Air inlet nozzles position above the throat (cm)		
	8	10	12
H_2	27.75	31.23	27.19
CO	27.59	24.99	23.83
CO_2	14.39	14.38	14.44
CH_4	3.75	3.20	2.59

It can be observed that the air inlet position had a significant effect on the concentration of H_2, CO and CH_4, but no influence on the CO_2 concentration. The ratio of H_2/CO increased from 1.01 to 1.25 and decreased to 1.14 when increasing the air inlet nozzles position above the throat. The concentration of CH_4 decreased from 3.75%mol to 2.59%mol, with increase in air inlet position from 8 cm to 12 cm above the throat, while

388 the concentration of CO_2 remained constant at 14.4%mol with all tested air inlet nozzles
389 position. These results can be explained because increasing the height of the air inlet
390 nozzles position above the throat results in a reduction in the length of the pyrolysis zone,
391 therefore the formation of CH_4 in this region was decreased. At the same time, increasing
392 the length of the reduction zone results in an increase the reaction time (Reactions R-4-
393 8), leading to an increases in concentrations of H_2 and CO and a reduction of CH_4
394 concentration. The maximised ratio of H_2/CO obtained in this study (Table 4) were in
395 good agreement with experimental data obtained in a small scale throat downdraft gasifier
396 at a fixed position of the air inlet nozzles at 10 cm above the throat [60-62]. However, the
397 experimental results obtained from Wim et al. [63] showed that the ratio of H_2/CO was
398 maximised at the position of the air inlet nozzles at 12.5 cm above the throat for a small
399 scale throat downdraft gasifier. It is known that the ratio of H_2/CO in the syngas has a
400 significant impact on its utilization i.e. $H_2/CO \leq 1$ is suitable for heating and power
401 generation in a small-scale heat engines (< 2MW) while the ratio of $H_2/CO > 1$ can be
402 used in the production of fuel or for chemical synthesis [64-66]. From Table 4, it can be
403 concluded that high quality syngas with a high ratio of H_2/CO at 1.25 and low
404 concentrations of CO_2 and CH_4 in the gas stream was obtained at the position of the air
405 inlet nozzles at 10 cm above the throat.

406 **3.2.2 Temperature profile**

407 The temperature distribution across the throat downdraft gasifier under various air inlet
408 nozzles positions located at 8, 10 and 12 cm above the throat at a fixed throat to gasifier
409 diameter ratio of 0.40 is illustrated in Figure 8. The position of the air inlet nozzles had
410 no significant effect on the temperature distribution in the pyrolysis and reduction zones.
411 However, the temperature was more uniform across the oxidation zone at a position of 10

and 12 cm (Figure 8b and 8c) than 8 cm above the throat (Figure 8a). This is because the position of the air inlet nozzles at 8 cm above the throat was located at the inclination of the throat, causing cold spots in the oxidation zone, therefore resulting in low and non-uniform temperature. Low and non-uniform temperature in the oxidation zone (< 1273 K) leads to a considerable amount of large molecular weight species (tar) in the gas stream [14, 17, 27, 67, 68]. If the rapid released of volatiles from the pyrolysis zone and gasifying agent are not well-mixed with gasifying agent and the temperature is not high enough for the cracking of tar compounds, there are difficulties for the downstream process such as corrosion, clogging and fouling of the installation. [15, 16].

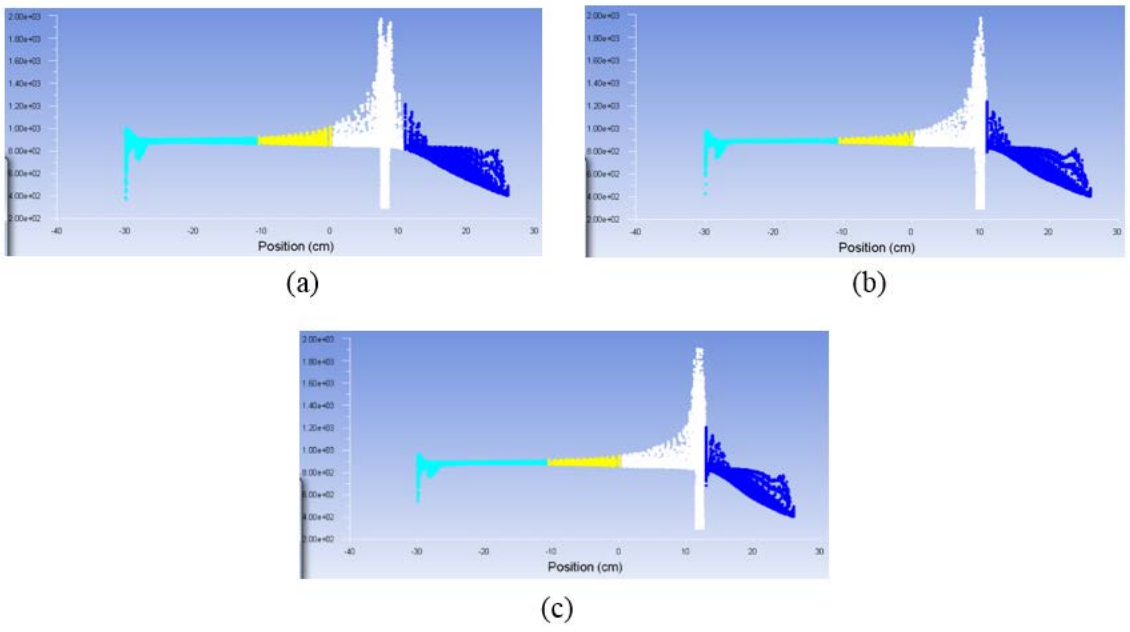

Figure 8: Temperature distribution at the air inlet nozzles position at (a) 8 cm; (b) 10 cm and (c) 12 cm above the throat at a fixed throat to gasifier diameter ratio of 0.40

4. Conclusions

A 20 cm diameter throat downdraft gasifier was designed and numerically optimised using the Computational Fluid Dynamic (CFD), ANSYS FLUENT 16.1. The produced gas composition and temperature distribution across the throat downdraft gasifier were

predicted and validated over various ratios of throat to gasifier diameter of 0.25-0.50 and the positions of the air inlet nozzles at 8, 10 and 12 cm above the throat. The modelling results showed that throat to gasifier diameter ratios and the position of the air inlet nozzles had a significant effect on the syngas formation, properties of gas and temperature distribution particularly in the oxidation zone. Increasing a ratio of throat to gasifier diameter decreased CH_4 concentration but had no effect on CO_2 formation. The highest concentration of H_2 and H_2/CO ratio (31.2%mol) at the ratio of H_2/CO (1.25) was obtained at a throat to gasifier diameter ratio of 0.40. Increasing further the ratio of throat to gasifier diameter caused a reduction in hydrogen or ratio of H_2/CO. Increasing the air inlet position from 8 cm to 10 cm above the throat increased the ratio of H_2/CO from 1.01 to 1.25. A further increase in the air inlet nozzle caused a reduction of H_2/CO to 1.14. A 31% reduction in the concentration of CH_4 was observed when increasing the air inlet nozzles from 8 cm to 12 cm above the throat.

A very good agreement between experimental and modelling data was observed, with less than 5% difference. The trend in temperature distribution in the gasifier obtained from the modelling was also in good agreement with experimental data. High and uniform temperature across the oxidation zone was also obtained at a throat to gasifier diameter ratio of 0.40. Therefore, the mathematical approach in this study can be used as a design and optimisation tools for a throat downdraft biomass gasifier to achieve high quality of syngas production. It also can be extended to predict the syngas compositions under the various operating conditions in a fixed throat downdraft gasifier i.e. different types of biomass feedstock, the equivalence ratio (ER).

References

[1] International Energy Outlook 2016 (IEO2016). International Energy Outlook 2016 with Projections to 2040, U.S. Energy Information Administration, DOE/EIA-0484, Washington, DC, 2016.

[2] International Energy Agency 2015 (IEA2015). Would Energy Outlook 2015, OECD/IEA, Paris, 2015.

[3] International Energy Agency (2000). World Energy Outlook 2000, IEA, Paris, 2000.

[4] IEA Bioenergy (2009). Bioenergy – a Sustainable and Reliable Energy Source – A Review of Status and Prospects (EXCO: 2009: 06).

[5] IEA Bioenergy (2015). Annual Report 2015 (EXCO: 2016: 0.1).

[6] Abhishek Sharma, Vishnu Pareek and Donke Zhang (2015). Biomass pyrolysis – A review of modelling, process parameters and catalytic studies. Renewable and Sustainable Energy Reviews, Volume 50, Pages 1081-1096.

[7] Ruiz, J.A., Juarez, M.C., Morales, M.P., Munoz, P. and Mendivil, M.A. (2013). Biomass gasification for electricity generation: Review of current technology barriers. Renewable and Sustainable Energy, Volume 18, Pages 174-183.

[8] Maria Puig-Arnavat, Joan Carles Vruno and Alberto Coronas (2010). Review and analysis of biomass gasification models. Renewable and Sustainable Energy Reviews, Volume 14, Issue 9, Pages 2841-2851.

[9] Aly Moustafa Radwan (2012). An overview on gasification of biomass for production of hydrogen rich gas. Pelagia Research Library, Volume 3, Pages 323-335.

[10] Yashwant Kumar (2015). Biomass gasification – A review. International Journal of Engineering Studies and Technical Approach, Volume 1, Pages 12-27.

475 [11] Frederic Fabry, Christophe Rehmet, Vandad-Julien Rohani and Laurent Fulcheri
476 (2013). Waste Gasification by Thermal Plasma: A Review. Waste and Biomass
477 Valorization, Volume 4, Issue 3, Pages 421-439.
478 [12] Li C. and Suzuki K. (2009). Tar property, analysis, reforming mechanism and model
479 for biomass gasification- An overview. Renewable and Sustainable Energy Review,
480 volume 13, Pages 594-604.
481 [13] Morf P. (2001) Secondary reactions of tar during thermochemical biomass
482 conversion. PhD thesis. Swiss Federal Institute of Technology, Zurich.
483 [14] Milne T., Evans R. and Abatzoglou (1998). Biomass Gasifier "Tars": Their Nature,
484 Formation and Conversion. National Renewable Energy Laboratory.
485 [15] Umberto Arena (2012). Process and technological aspects of municipal solid waste
486 gasification. A review. Waste Management, Volume 32, Issue 4, Pages 625-639.
487 [16] Linghong Zhang, Chunbao Xu and Pascale Champagne (2010). Overview of recent
488 advances in thermos-chemical conversion of biomass. Energy Conversion and
489 Management, Volume 51, Issue 5, Pages 969-982.
490 [17] Shanhui Zhao, Yi Su, Wenguang Wu, Yunliang Zhange, Yuu Wang and Yonghao
491 Luo (2013). Numerical Simulation of Partial Combustion for Biomass Tar Elimination in
492 Two-Stage Gasifier. Journal of Sustainable Bioenergy Systems, Volume 3, Pages 86-92.
493 [18] Xinging Lan, Hanbin Zhong and Jinsen Gao (2014). CFD simulation on the
494 gasification of asphalt water slurry in an entrained flow gasifier. Petroleum Science,
495 Volume 11, Issue 2, Pages 308-317.
496 [19] Pubet Meenaroch, Somrat Kerdsuwan and Krongkaew Laohalidanond (2015).
497 Development of Kinetics Models in Each Zone of a 10 Kg/hr Downdraft Gasifier using
498 Computational Fluid Dynamics. Energy Procedia, Volume 79, Pages 278-283.

499 [20] Ashish Chaurasia (2016). Modeling, simulation and optimization of downdraft
500 gasifier: Studies on chemical kinetics and operating conditions on the performance of the
501 biomass gasification process. Energy, Volume 116, Part 1, Pages 1065-1076.
502 [21] Ozgun Yucel and Mehmet Alaittin Hastaoglu (2016). Kinetic modelling and
503 simulation of throat downdraft gasifier. Fuel Processing Technology, Volume 144, Pages
504 145-154.
505 [22] Nuno Couto, Valter Silva, Eliseu Monteiro, Paulo Brito and Abel Rouboa (2015).
506 Using an Eulerian-granular 2-D multiphase CFD model to simulate oxygen air enriched
507 gasification of agroindustrial residues. Renewable Energy, Volume 77, Pages174-181.
508 [23] Dejtrakulwong C. and Patumsawad S. (2014). Four Zones modelling of the
509 Downdraft Biomass Gasification Process: Effect of Moisture Content and Air to Fuel
510 ratio. Energy Procedia, Volume 52, Pages 142-149.
511 [24] Yueshi Wu, Qinglin Zhang, Weihong Yang and Wlodzimierz Blasiak (2013). Two-
512 Dimensional Computational Fluid Dynamics Simulation of Biomass Gasification in a
513 Downdraft Fixed-Bed Gasifier with Highly Preheated Air and Steam. Energy and Fuels,
514 Volume 27, Pages 3274-3282.
515 [25] Keran D. Patel, N.K. Shah and R.N, Patel (2013). CFD Analysis of Spatial
516 Distribution of Various Parameters in Downdraft Gasifier. Procedia Engineering, Volume
517 51, Pages 764-769.
518 [26] Muilenburg M. (2011). Computational modelling of the combustion and gasification
519 zones in a downdraft gasifier. Master Thesis lowa University.
520 [27] Luc Gerun, Maria Paraschiv, Razvan Vijeu, Jerome Bellettre, Mohand Tazerout,
521 Benny Gobel and Ulrik Henriksen (2008). Numerical investigation of the partial
522 oxidation in a two-stage downdraft gasifier. Fuel, Volume 87, Issue 7, Pages 1383-1393.

523 [28] Rogel A. and Aguillon J. (2006). The 2D Eulerian Approach of Entrained Flow and
524 Temperature in a Biomass Stratified Downdraft Gasifier. American Journal of Applied
525 Sciences, Volume 3, Pages 2068-2078.
526 [29] Zainal Z.A., Ali Rifau, Quadir and Seetharamu K.N. (2002). Experimental
527 investigation of a downdraft biomass gasifier. Biomass and Bioenergy, Volume 23, Pages
528 283-289.
529 [30] Sivakumar S., Pitchandi K. and Natarajan E. (2006). Design and Analysis of
530 DownDraft Biomass Gasifier using Computational Fluid Dynamics. Department of
531 Mechanical Engineering, College of Engineering, Guindy, Anna, INDIA.
532 [31] Rivi Kumar, Narendhar Baba, Suresh Kumar and Venkata Vishnu (2016). CFD
533 Simulation of Down Draft Biomass Gasifier. International Journal of Advance
534 Engineering and Research, Volume 3, Issue 1.
535 [32] Jayah T.H., Lu Aye, Fuller R.J. and Stewart D.F. (2003). Computer simulation of a
536 downdraft wood gasifier for tea drying. Biomass and Bioenergy, Volume 25, Pages 459-
537 469.
538 [33] Sivakumar S., Pitchandi K. and Natarajan E. (2008). Modelling and simulation of
539 down draft wood gasifier. Journal of Applied Science, Volume 8, Issue 2, Page 271-279.
540 [34] Dziyad Dzulfansyah, Leopold Oscar Nelwan and Dyah Wulandani (2014).
541 Computational Fluid Dynamic Analysis for Desiging Downdraft-Rice Hush Gasifier.
542 Journal Keteknikan Pertanian, Volume 2, Pages 133-140.
543 [35] Gerber S., Behrendt F. and Oevermann M. (2010). An Eulerian modelling approach
544 of wood gasification in a bubbling fluidized bed reactor using char as bed material. Fuel,
545 Volume 89, Pages 2903-2917.

546 [36] Haojie Fan, Dengfei Mei, Fengguo Tian, Xuan Cui and Mingchuan Zhang (2016).
547 DEM simulation of different particle ejection mechanisms in a fluidized bed with and
548 without cohesive interparticle forces. Powder Technology, Volume 288, Pages 228-240.
549 [37] Xiaofang Wang, Baosheng Jin and Wenqi Zhong (2009). Three-dimensional
550 simulation of fluidized bed coal gasification. Chemical Engineering and Processing:
551 Process Intensification, Volume 48, Pages 695-705.
552 [38] Yuqing Feng, Tim Swenser-Smith, Peter J. Witt, Christian Doblin, Seng Lim and M.
553 Phil Schwarz (2012). CFD modelling of gas-solid flow in an internally circulating
554 fluidized bed. Powder Technology, Volume 219, Pages 78-85.
555 [39] Xiaoke Ku, Tian Li and Terese Lovas (2015). CFD-DEM simulation of biomass
556 gasification with steam in a fluidized bed reactor. Chemical Engineering Science, Volume
557 122, Pages 270-283.
558 [40] Liang Lu, T.M. Ismail, Yuqi Jin, M. Abd EI-Salam and Kunio Yoshikawa (2016).
559 Numerical and experimental investigation on co-combustion characteristics of
560 hydrothermally treated municipal solid waste with coal in a fluidized bed. Fuel Processing
561 Technology, Volume 154, Pages 52-65.
562 [41] Shafie S.M., Mahlia T.M.I., Masjuki H.H. and Ahmad-Yazid A. (2012). A review
563 on electricity generation bases on biomass residue in Malaysia. Renewable and
564 Sustainable Energy Reviews, Volume 16, Issue 8, Pages 5879-5889.
565 [42] Niranjan Fernando and Mahinsasa Narayana (2016). A comprehensive two
566 dimensional Computational Fluid Dynamics model for an updraft biomass gasifier.
567 Renewable Energy, Volume 99, Pages 698-710.

568 [43] Wahab Mojtahedi, Matti Ylitalo, Teuvo Maunula and Javad Abbasian (1995).
569 Catalytic decomposition of ammonia in fuel gas produced in pilot-scale pressurized
570 fluidized-bed gasifier. Fuel Processing Technology, Volume 45, Issue 3, Pages 211-236.
571 [44] Pekka Simell, Esa Kurkela, Pekka Stahlberg and Jouko Hepola (1996). Catalytic hot
572 gas cleaning of gasification gas, Catalysis Today, Volume 27, Issues 1-2, Pages 55-62.
573 [45] Lopamudra Devi, Krzysztof J. Ptasinski and Frans J.J.G. Jamssen (2003). A review
574 of the primary measures for tar elimination in biomass gasification processes. Biomass
575 and Bioenergy, Volume 24, Issue 2, Pages 125-140.
576 [46] Colomba Di Blasi (2000). Dynamic behaviour of stratified downdraft gasifier.
577 Chemical Engineering Science, Volume 55, Pages 2931-2944.
578 [47] Colomba Di Blasi (2008). Modeling chemical and physical processes of wood and
579 biomass pyrolysis. Progress in Energy and Combustion Science, Volume 34, Pages 47-
580 90.
581 [48] Fernando N., Amin M., Narayana M., Jayawickrama T. and Jayasena S. (2015). A
582 mathematical model for pyrolysis of biomass. Moratuwa Eng. Res. Conf. (MERCon),
583 IEEE Conference 2015.
584 [49] Chan WR, Kelbon M and Krieger BB (1985). Modeling and experimental
585 verification of physical and chemical processes during pyrolysis of large biomass particle.
586 Fuel, Volume 64, Pages 1505-1513.
587 [50] Prabir Basu (2010). Gasification theory and modelling of gasifiers. In: Biomass
588 Gasification design Handbook. Academic Press, Boston.
589 [51] Marco Simone, Cristiano Nicolella and Leonardo Tognotti (2013). Numerical and
590 experimental investigation of downdraft gasification of woody residues. Bioresource
591 Technology, Volume 133, Pages 92-101.

592 [52] Janajreh I. and Al Shrah M. (2013). Numerical and experimental investigation of
593 downdraft gasification of wood chips. Energy Conversion and Management, Volume 65,
594 Pages 783-792.
595 [53] Yueshi Wu, Weihong Yang and Wlodzimierz Blasiak (2014). Energy and Exergy
596 Analysis of High Temperature Agent Gasification of Biomass. Energies, Volume 7, Pages
597 2107-2122.
598 [54] Chawdhury M.A. and Mahkamov K. (2011). Development of a Small Downdraft
599 Biomass Gasifier for Developing Countries. Journal of Scientific Research, Volume 3,
600 Pages 51-64.
601 [55] Duleeka Gunarathne, Sumudu Sajeewareka Jatunarachchi, Nihal srikantha
602 Senanayake and Bo Wei (2013). The effect of Throat Diameter on the Performance a
603 Downdraft Biomass Gasifier. International Journal of Energy Engineering, Volume3,
604 Pages 171-175.
605 [56] Kinoshita C. Turn S., Overend R. and Bain R. (1997). Power generation potential of
606 biomass gasification systems. Journal of Energy Engineering, Volume 123, Issue 3, Pages
607 88-99.
608 [57] Rolando Zanzi, Krister Sjostrom and Emilia Bjornbom (2002). Rapid pyrolysis of
609 agricultural residues at high temperature. Biomass and Bioenergy, Volume 23, Issue 5,
610 Pages 357-366.
611 [58] Pfeifer C., Rauch R. and Hofbauer H. (2004). In-Bed Catalytic Tar reduction in a
612 Dual Fluidized Bed Biomass steam Gasifier. Industrial and Engineering Chemistry
613 Research, Volume 43, Issue 7, Pages 1634-1640.

614 [59] Chuang-zhi Wu, Xiu-li Yin, Long-long Ma, Zhao-qiu Zhou and Han-ping Chen
615 (2009). Operational characteristics of a 1.2-MW biomass gasification and power
616 generation plant. Biotechnology Advances, Volume 27, Pages 588-592.
617 [60] Jan Venselaar (1982). Design rules for down draft wood gasifiers – A short review.
618 Project JTA-9A – Research Development at Institute Technology Bandung, Indonesia.
619 [61] FAO (1986). Wood gas as engine fuel. FAO Forestry Paper 72, Rome, Italy (UN-
620 FAO Forestry Department).
621 [62] Adenike A. Kolawole, S.B. Adeyemo and Moradeyo K. Odunfa (2013). Design and
622 Construction of Wood Gasifier, Mechanical Engineering Department, University of
623 Ibadan,Nigeria,http://www.academia.edu/7724922/design_and_construction_of_wood_
624 gasifier [accessed 13.01.17].
625 [63] Wim P.M. van Swaaij, Sascha R.A. Kersten and Wolfgang Palz (2015).
626 Transformations to Effective Use Biomass Power for the World. Pan Stanford Series on
627 Renewable Energy Volume 6. In: Biomass Gasification System for small-Scale Power
628 Generation: Design Rules and Considerations for Systems Including the Down-Draft
629 Gasifier.
630 [64] Yung M.M., Jablonski W.S. and Magrini-Bair K.A. (2009). Review of Catalytic
631 Condition of biomass-Derived Syngas. Energy and Fuels, Volume 23, Issue 4, Pages
632 1874-1887.
633 [65] Torres W., Pansare S. and Goodwin J. (2007). Hot gas removal of tars, ammonia and
634 hydrogen sulphide from biomass gasification tars. Catalysis Reviews, Volume 49, Pages
635 407-456.

636 [66] Chaudhari S.T., Bej S.K., Bakhshi N.N. and Dalai A.K. (2001). Steam gasification
637 of biomass-derived char for the production of carbon monoxide-rich synthesis gas.
638 Energy and Fuel, Volume 15, Pages 736-742.
639 [67] McKendry P. (2002). Energy production from biomass (part 3): Overview of
640 biomass. Bioresource Technology, Volume 83, Pages 55-63.
641 [68] Morf P., Hasler P. and Nussbaumer T. (2002). Mechanisms and kinetics of
642 homogeneous secondary reactions of tar from continuous pyrolysis of wood chips, Fuel,
643 Volume 81, Pages 843-853.